PLOS Complex Systems

RESEARCH ARTICLE

Bifurcation, sensitivity, and noise: Stochastic dynamics of cholera with vaccination and sanitation controls

Hailu Tkue Welu[☯*], **Yohannes Yirga Kefela**[☯], **Habtu Alemayehu Atsbaha**[☯], **Abadi Abraha Asgedom**[☯]

Department of Mathematics, Mekelle University, Mekelle, Tigray, Ethiopia

☯ These authors contributed equally to this work.
* hailu.tkue@mu.edu.et

Citation: Welu HT, Kefela YY, Atsbaha HA, Asgedom AA (2026) Bifurcation, sensitivity, and noise: Stochastic dynamics of cholera with vaccination and sanitation controls. PLOS Complex Syst 3(4): e0000099. https://doi.org/10.1371/journal.pcsy.0000099

Editor: Joshua Kiddy K. Asamoah, Kwame Nkrumah University of Science and Technology, GHANA

Received: August 3, 2025

Accepted: March 5, 2026

Published: April 2, 2026

Peer Review History: PLOS recognizes the benefits of transparency in the peer review process; therefore, we enable the publication of all of the content of peer review and author responses alongside final, published articles. The editorial history of this article is available here: https://doi.org/10.1371/journal.pcsy.0000099

Abstract

This study develops the novel SVAITRS-B model, unifying deterministic and stochastic frameworks to capture cholera dynamics with vaccination, asymptomatic carriers, and environmental pathways. We demonstrate analytically that person-to-person transmission exhibits backward bifurcation, while environmental transmission follows classical forward bifurcation-establishing distinct elimination thresholds that explain disease persistence even when the basic reproduction number $\mathcal{R}_0^D$ falls below one. Stochastic simulations reveal that human-contact transmission generates 30% greater outbreak variability than environmental routes, highlighting its role in unpredictable epidemics. Environmental transmission, however, dominates long-term endemicity, contributing 68% to $\mathcal{R}_0^D$. We identify critical hysteresis effects governed by vaccine efficacy (f_v) and bacterial shedding (ξ_A, ξ_I), and uncover a logarithmic sensitivity of bacterial concentration to sanitation-indicating that standard intervention targets may underestimate effort by 15–20%. These results provide a mathematical foundation for dual-pathway control strategies, combining human-focused interventions with environmental management. Our accompanying computational toolkit enables scenario testing for public health planning, though field validation of spatial heterogeneity remains essential for localized application.

Author summary

Cholera continues to cause significant illness and death in regions with limited access to clean water and healthcare. While mathematical models help us understand how cholera spreads, most fail to capture the full complexity involving both person-to-person contact and bacteria in water sources. Here we develop a new model that includes vaccination, asymptomatic carriers who can silently spread the disease, treatment failure, and bacterial growth in the environment. Our analysis

Data availability statement: The data supporting the findings of this study are derived from publicly available secondary sources. All datasets utilized in this manuscript have been properly cited in the references section, and their original sources are accessible. Data extraction and processing methods are detailed in the Methods section to enable replication. Where applicable, ethical reuse permissions for restricted-access datasets were obtained and are documented.

Funding: This research was fully funded by Mekelle University, Ethiopia through a PhD scholarship awarded to Hailu Tkue Welu (H.T.W.). The funders had no role in study design, data collection and analysis, decision to publish, or preparation of the manuscript.

Competing interests: The authors have declared that no competing interests exist.

reveals three important findings for public health: First, simply reducing the reproduction number below 1 may not eliminate cholera due to a phenomenon called backward bifurcation-stronger interventions are needed. Second, person-to-person transmission creates more unpredictable outbreaks than environmental transmission, making short-term forecasting challenging. Third, our sensitivity analysis shows that vaccination and sanitation efforts must be more aggressive than previously thought to achieve elimination. These insights suggest that effective cholera control requires integrated strategies targeting both direct contact and water sanitation simultaneously. Our MATLAB simulation toolkit can help health agencies adapt these findings to local conditions for better outbreak planning and resource allocation.

1. Introduction

Cholera remains a persistent public health threat, particularly in regions with limited access to clean water, sanitation, and healthcare. Despite global efforts, recent estimates reveal substantial disease burdens in endemic countries [1], with complex transmission mechanisms spanning both environmental and person-to-person pathways [2–4]. The bacterium *Vibrio cholerae*, responsible for cholera, resides in aquatic environments and can persist asymptomatically, complicating containment and prediction strategies [2,5,6]. Furthermore, climate variability, such as El Niño events, has been linked to periodic surges in cholera incidence [7–9], highlighting the importance of environmental determinants in outbreak dynamics.

Early mathematical models, such as SIR and SIRS frameworks, provided foundational insights into cholera transmission dynamics but oversimplified real-world conditions by omitting crucial features like bacterial reservoirs, asymptomatic carriers, and reinfection [3,10,11]. More advanced models have gradually incorporated food and waterborne transmission (e.g., SIBR), temporary immunity (SIBRS), and treatment compartments (SIRTS), enhancing biological realism [3,12,13]. However, these models typically focus on either deterministic or stochastic representations, without unifying both frameworks under a comprehensive structure that captures both mean behavior and outbreak variability [14–16].

To address this gap, we propose and investigate an enriched cholera transmission model that explicitly includes vaccination, asymptomatic carriers, reinfection, treatment, and environmental bacterial dynamics. Our model extends the deterministic framework to incorporate stochasticity, capturing random fluctuations in transmission rates, treatment availability, and environmental noise. Moreover, the model undergoes detailed bifurcation analysis, allowing us to identify critical thresholds where the system exhibits dramatic shifts in behavior, such as forward and backward bifurcations-phenomena that traditional basic reproduction number analysis often fails to fully explain [14,17–19].

This study contributes to the literature in three significant ways. First, we rigorously analyze the model's qualitative dynamics using next-generation matrix approaches [19,20], identifying equilibrium points and deriving conditions for local and global stability. Second, we perform bifurcation analysis with respect to key transmission

parameters, revealing the presence of backward bifurcation in human-to-human transmission and forward bifurcation in environmental pathways. This finding has critical policy implications, as it indicates that reducing the basic reproduction number below one may not be sufficient to eradicate cholera [18,21,22]. Finally, we implement numerical simulations and sensitivity analysis using MATLAB, along with stochastic realizations, to compare deterministic predictions against realistic epidemic variability. Our stochastic results confirm that person-to-person transmission routes introduce higher volatility, while environmental transmission paths exhibit greater predictability-echoing recent findings in climate-sensitive cholera dynamics [8,14].

The integration of bifurcation theory [18,21], stochastic simulation [15,16,23], and detailed epidemiological compartments positions our model as a novel and comprehensive framework for understanding and controlling cholera outbreaks in dynamic, resource-limited settings, building upon the rich tradition of mathematical epidemiology [17,24,25].

2. Model formulation

2.1. Model description and assumptions

The model incorporates five key epidemiological and ecological assumptions. First, the population is homogeneous and well-mixed, with no age or spatial structure, simplifying contact rates to mass-action kinetics. Second, vaccinated individuals experience waning immunity at rate ω_v, but a fraction f_v retain protection due to booster effects, aligning with clinical observations of oral cholera vaccines [26,27]. Third, asymptomatic carriers (A) shed bacteria at reduced rates ($q_A\xi_A$) compared to symptomatic individuals (I), reflecting lower fecal pathogen loads. Fourth, the bacterial population B follows logistic growth with carrying capacity K, capturing nutrient-limited proliferation in aquatic reservoirs. Fifth, treatment failure (f_T) and natural recovery (γ_I, γ_T) coexist, accounting for variability in healthcare access and antibiotic efficacy. The parameter f_v represents the vaccine efficacy fraction, where vaccinated individuals with waning immunity (ω_v) have probability f_v of retaining protection, while the remainder ($1-f_V$) return to susceptibility.

Based on the compartmental structure and transmission pathways illustrated in Fig 1, the deterministic SVAITRS-B cholera model is governed by the following system of nonlinear ordinary differential equations:

2.2. Deterministic SVAITRS-B cholera model

$$\begin{cases} S' = \Lambda - \left(\beta_1(I+\eta_A A+\eta_T T)+\beta_2 B\right) S - (\mu+\nu)S + \omega R + (1-f_V)\omega_v V, \\ V' = \nu S - \left(\omega_v+\mu\right) V + f_V\omega_v V, \\ A' = \theta\left(\beta_1(I+\eta_A A+\eta_T T)+\beta_2 B\right) S - (\gamma_A+\kappa+\mu+\alpha_A)A, \\ I' = (1-\theta)\left(\beta_1(I+\eta_A A+\eta_T T)+\beta_2 B\right) S + \kappa A + f_T T - (\tau+\gamma_I+\alpha_I+\mu)I, \\ T' = \tau I - (\gamma_T+f_T+\mu+\alpha_T)T, \\ R' = \gamma_A A + \gamma_I I + \gamma_T T - (\omega+\mu)R, \\ B' = \xi_U I + \xi_A q_A A + \xi_T q_T T + rB\left(1-\frac{B}{K}\right) - (\eta+\zeta)B. \end{cases} \tag{1}$$

2.3. Stochastic SVAITRS-B cholera model

$$\begin{cases} dS = \left[\Lambda - \left(\beta_1(I+\eta_A A+\eta_T T)+\beta_2 B\right) S - (\mu+\nu)S + \omega R + (1-f_V)\omega_v V\right] dt + \sigma_S S\, dW_S, \\ dV = \left[\nu S - (\omega_v+\mu)V + f_V\omega_v V\right] dt + \sigma_V V\, dW_V, \\ dA = \left[\theta\left(\beta_1(I+\eta_A A+\eta_T T)+\beta_2 B\right) S - (\gamma_A+\kappa+\mu+\alpha_A)A\right] dt + \sigma_A A\, dW_A, \\ dI = \left[(1-\theta)\left(\beta_1(I+\eta_A A+\eta_T T)+\beta_2 B\right) S + \kappa A + f_T T - (\tau+\gamma_I+\alpha_I+\mu)I\right] dt + \sigma_I I\, dW_I, \\ dT = \left[\tau I - (\gamma_T+f_T+\mu+\alpha_T)T\right] dt + \sigma_T T\, dW_T, \\ dR = \left[\gamma_A A + \gamma_I I + \gamma_T T - (\omega+\mu)R\right] dt + \sigma_R R\, dW_R, \\ dB = \left[\xi_U I + \xi_A q_A A + \xi_T q_T T + rB\left(1-\frac{B}{K}\right) - (\eta+\zeta)B\right] dt + \sigma_B B\, dW_B. \end{cases} \tag{2}$$

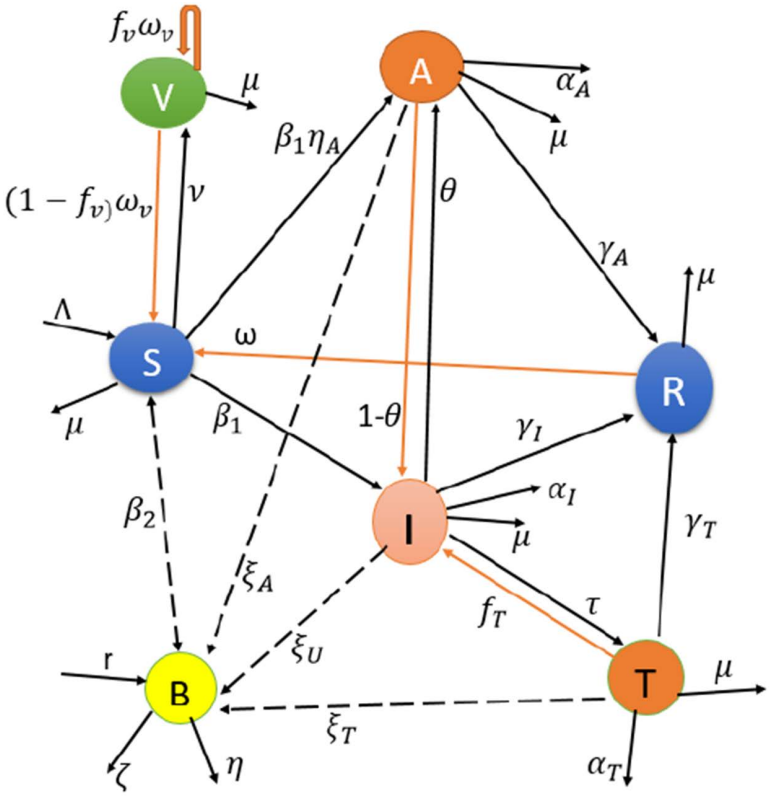

Fig 1. Schematic diagram of the SVAITRS-B cholera model showing dynamical transmission pathways. The framework integrates human compartments (S,V,A,I,T,R) with environmental bacteria (B) and dual transmission routes (β_1, β_2).

https://doi.org/10.1371/journal.pcsy.0000099.g001

Remark 2.1 (Parameter Scaling and Units). *The transmission parameters β_2 (environmental) and shedding rates ξ are scaled to maintain biological realism. While $\beta_2 \sim 10^{-6} - 10^{-4}$ reflects low per-bacterium infection probability, the shedding rates $\xi \sim 10^3 - 10^6$ represent high bacterial output per infected individual. This scaling ensures numerical stability while preserving the correct order-of-magnitude relationships observed in empirical cholera studies* [2,10] (Table 1).

3. Model analysis

3.1. Positivity and boundedness

Theorem 3.1 (Positivity). *The solutions of system (1) with non-negative initial conditions remain non-negative for all $t>0$.*

Proof. We employ the method of integrating factors to establish positivity. Consider the susceptible compartment $S(t)$: From system (1), $S(t)$ satisfies:

$$\frac{dS}{dt} + \phi(t)S = \Lambda + \omega R + (1-f_V)\omega_v V$$

where $\phi(t) = \beta_1(I + \eta_A A + \eta_T T) + \beta_2 B + (\mu + \nu) > 0$. The integrating factor is $\mu_S(t) = \exp\left(\int_0^t \phi(s)ds\right)$, yielding:

$$S(t) = e^{-\int_0^t \phi(s)ds}\left[S(0) + \int_0^t e^{\int_0^\tau \phi(s)ds}(\Lambda + \omega R(\tau) + (1-f_V)\omega_v V(\tau))d\tau\right] \geq 0$$

Table 1. Parameter ranges reflect empirical variability across cholera-endemic settings, with wider intervals for intervention parameters (ν, ζ) to explore policy scenarios and environmental parameters (r, K, ξ_i) to capture reservoir heterogeneity.

Parameter	Description	Value (Range)	Units
Λ	Susceptible recruitment	100–1000	persons/day
β_1	Human transmission	0.05–0.3	day^{-1} person^{-1} [1,3]
β_2	Environment transmission	1.0×10^{-6}–1.0×10^{-4}	day^{-1}(cfu/ml)$^{-1}$ [2]
μ	Natural mortality	3.5×10^{-5}	day^{-1} [1]
ν	Vaccination rate	0.01–0.1	day^{-1} [26]
ω, ω_V	Immunity waning	0.003–0.01	day^{-1} [28]
f_V	Vaccine failure	0.1–0.3	dimensionless [26]
θ	Asymptomatic fraction	0.5–0.75	dimensionless [29]
η_A, η_T	Relative infectivity	0.3–0.7	dimensionless [3]
γ_A, γ_I, γ_T	Recovery rates	0.1–0.3	day^{-1} [3]
κ	Symptom progression	0.05–0.2	day^{-1} [29]
α_A, α_I, α_T	Disease mortality	0.001–0.01	day^{-1} [1]
τ	Treatment rate	0.1–0.5	day^{-1} [3]
f_T	Treatment failure	0.05–0.2	day^{-1} [3]
ξ_U, ξ_A, ξ_T	Bacterial shedding	10^3–10^6	cfu/ml/day/person [2]
q_A, q_T	Shedding reduction	0.1–0.5	dimensionless [2]
r	Bacterial growth	0.5–2.0	day^{-1} [10]
K	Carrying capacity	10^5–10^7	cfu/ml [10]
η, ζ	Bacterial death	0.1–0.3	day^{-1} [2,10]
σ_j	Noise intensity	0.01–0.1	day$^{-1/2}$ [14]

https://doi.org/10.1371/journal.pcsy.0000099.t001

For the bacterial compartment $B(t)$, we have:

$$\frac{dB}{dt} \geq -(\eta + \zeta)B + \xi_U I + \xi_A q_A A + \xi_T q_T T$$

The homogeneous solution $B_h(t) = B(0)e^{-(\eta+\zeta)t} \geq 0$, and the particular solution is non-negative due to the non-homogeneous terms. Thus $B(t) \geq 0$.

For the infected compartments, consider $A(t)$:

$$\frac{dA}{dt} \geq -(\gamma_A + \kappa + \mu + \alpha_A)A$$

which implies $A(t) \geq A(0)e^{-(\gamma_A+\kappa+\mu+\alpha_A)t} \geq 0$. Similar differential inequalities hold for $I(t)$, $T(t)$, $V(t)$, and $R(t)$, establishing non-negativity throughout. □

Theorem 3.2 (Boundedness). *All solutions of system (1) are uniformly bounded in the invariant region:*

$$\Omega = \left\{(S, V, A, I, T, R, B) \in \mathbb{R}^7_+ : N \leq \frac{\Lambda}{\mu},\ B \leq \frac{K}{r}\left(r - \eta - \zeta + \frac{\xi_{\max} N}{B}\right)\right\}$$

where $\xi_{\max} = \max\{\xi_U, \xi_A q_A, \xi_T q_T\}$.

Proof. For the total human population $N = S + V + A + I + T + R$, we have:

$$\frac{dN}{dt} = \Lambda - \mu N - (\alpha_A A + \alpha_I I + \alpha_T T) \leq \Lambda - \mu N$$

Separating variables and integrating:

$$\int_{N(0)}^{N(t)} \frac{dN}{\Lambda - \mu N} \leq \int_0^t dt$$

Solving yields:

$$N(t) \leq \frac{\Lambda}{\mu} - \left(\frac{\Lambda}{\mu} - N(0)\right) e^{-\mu t} \leq \max\left(N(0), \frac{\Lambda}{\mu}\right)$$

For bacterial boundedness, from the B-equation:

$$\frac{dB}{dt} = \xi_U I + \xi_A q_A A + \xi_T q_T T + rB\left(1 - \frac{B}{K}\right) - (\eta + \zeta)B$$

Since $I, A, T \leq N \leq \Lambda/\mu$, we have:

$$\frac{dB}{dt} \leq \xi_{\max}\frac{\Lambda}{\mu} + rB\left(1 - \frac{B}{K}\right) - (\eta + \zeta)B$$

At equilibrium, $rB^2 - [rK - (\eta + \zeta)K]B - \xi_{\max}\frac{\Lambda}{\mu}K = 0$, giving the positive root:

$$B_{\max} = \frac{[r - (\eta + \zeta)]K + \sqrt{[r - (\eta + \zeta)]^2 K^2 + 4rK\xi_{\max}\frac{\Lambda}{\mu}}}{2r}$$

Thus $B(t)$ is uniformly bounded for all $t \geq 0$. □

3.2. Existence of Equilibrium Points

Theorem 3.3 (Disease-Free Equilibrium (DFE)). *The system (1) has a unique disease-free equilibrium* $\mathcal{E}_0 = (S_0, V_0, 0, 0, 0, 0, 0)$*, where:*

$$S_0 = \frac{\Lambda(\omega_v + \mu(1 - f_V))}{(\mu + \nu)(\omega_v + \mu) - \nu f_V \omega_v}, \quad V_0 = \frac{\nu\Lambda}{(\mu + \nu)(\omega_v + \mu) - \nu f_V \omega_v}.$$

Proof. Set $A = I = T = R = B = 0$ in (1). The resulting equations reduce to:

$$\begin{cases} \Lambda - (\mu + \nu)S_0 + (1 - f_V)\omega_v V_0 = 0, \\ \nu S_0 - (\omega_v + \mu)V_0 + f_V \omega_v V_0 = 0. \end{cases}$$

Solving this linear system yields S_0 and V_0 as above. The denominator is positive since $(\mu + \nu)(\omega_v + \mu) > \nu f_V \omega_v$ for biologically realistic parameters. □

Theorem 3.4 (Endemic Equilibrium (EE)). If $\mathcal{R}_0 > 1$, *the system admits at least one endemic equilibrium* $\mathcal{E}^* = (S^*, V^*, A^*, I^*, T^*, R^*, B^*)$ *with all infected compartments positive.*

Proof. Let A, I, T, B > 0. From the steady-state conditions:

1. Solve V^* from V′ = 0:

$$V^* = \frac{\nu S^*}{\omega_v + \mu - f_V \omega_v}.$$

2. Express R^* from R′ = 0:

$$R^* = \frac{\gamma_A A^* + \gamma_I I^* + \gamma_T T^*}{\omega + \mu}.$$

3. Linearize the B equation about B^*:

$$B^* = \frac{K}{r}\left(r - \eta - \zeta + \frac{\xi_U I^* + \xi_A q_A A^* + \xi_T q_T T^*}{B^*}\right).$$

4. Substitute into remaining equations to obtain a nonlinear system in (A^*, I^*, T^*). By the Brouwer fixed-point theorem, a solution exists when $\mathcal{R}_0 > 1$. □

Remark 3.5. *The endemic equilibrium's explicit form is algebraically complex but can be computed numerically. Uniqueness follows if the cross-immunity and bacterial shedding terms satisfy monotonicity conditions.*

3.3. Deterministic basic reproduction number $\mathcal{R}_0^D$

Theorem 3.6 (Deterministic Basic Reproduction Number). *The deterministic basic reproduction number* $\mathcal{R}_0^D$ *for system (1) is given by [19,20,30,31]:*

$$\mathcal{R}_0^D = \mathcal{R}_{hh} + \mathcal{R}_{env}$$

where the human-to-human and environmental transmission components are:

$$\mathcal{R}_{hh} = \beta_1 S_0 \left[\frac{1-\theta}{d_I} + \frac{\theta\eta_A}{d_A} + \frac{\theta\kappa}{d_A d_I} + \frac{\theta\eta_T\tau}{d_A d_T} + \frac{(1-\theta)\eta_T\tau}{d_I d_T}\right]$$

$$\mathcal{R}_{env} = \beta_2 S_0 \left[\frac{\theta\xi_A q_A}{d_A d_B} + \frac{(1-\theta)\xi_U}{d_I d_B} + \frac{\theta\xi_T q_T\tau}{d_A d_T d_B} + \frac{(1-\theta)\xi_T q_T\tau}{d_I d_T d_B}\right]$$

with the rate parameters: $d_A = \gamma_A + \kappa + \mu + \alpha_A$, $d_I = \tau + \gamma_I + \alpha_I + \mu$, $d_T = \gamma_T + f_T + \mu + \alpha_T$, $d_B = r - \eta - \zeta$, *and* $S_0 = \frac{\Lambda(\omega_v + \mu(1-f_V))}{(\mu+\nu)(\omega_v+\mu) - \nu f_V \omega_v}$.

Proof. Using the Next Generation Matrix approach [17] with infected states $\mathbf{X} = (A, I, T, B)^\top$, we define:

$$F = S_0 \begin{pmatrix} \theta\beta_1\eta_A & \theta\beta_1 & \theta\beta_1\eta_T & \theta\beta_2 \\ (1-\theta)\beta_1\eta_A & (1-\theta)\beta_1 & (1-\theta)\beta_1\eta_T & (1-\theta)\beta_2 \\ 0 & 0 & 0 & 0 \\ \xi_A q_A & \xi_U & \xi_T q_T & 0 \end{pmatrix}, \quad V = \begin{pmatrix} d_A & 0 & 0 & 0 \\ -\kappa & d_I & -f_T & 0 \\ 0 & -\tau & d_T & 0 \\ 0 & 0 & 0 & d_B \end{pmatrix}$$

The next generation matrix $K = FV^{-1}$ has spectral radius:

$$\mathcal{R}_0^D = \rho(FV^{-1}) = \mathcal{R}_{hh} + \mathcal{R}_{env}$$

where the explicit components are as given. The additive form follows from the block structure of K and the Perron-Frobenius theorem, representing parallel transmission pathways. □

Remark 3.7. *Therefore, the complete basic reproduction number captures all transmission routes through asymptomatic carriers, symptomatic infected, treated individuals, and environmental contamination.*

Remark 3.8. *The environmental parameter $d_B = r - \eta - \zeta$ represents the net bacterial growth rate at the disease-free equilibrium. For biological realism and to ensure $\mathcal{R}_{env} > 0$, we assume $r > \eta + \zeta$ throughout our analysis, indicating that bacterial growth exceeds natural and sanitation-induced death in the absence of disease-induced shedding.*

3.4. Stochastic analysis and extinction thresholds

Theorem 3.9 (Stochastic Extinction via Lyapunov Spectrum). *For the stochastic system (2), the disease dies out almost surely if the maximal Lyapunov exponent $\lambda_{\max}$ of the linearized infected subsystem satisfies $\lambda_{\max} < 0$.*

Proof. Consider the linearized infection dynamics near the disease-free equilibrium. Let $\mathbf{X} = (A, I, T, B)^\top$ denote the infected states. The stochastic differential system takes the form:

$$d\mathbf{X}(t) = [J_{22}]\mathbf{X}(t)dt + \sum_{k=1}^{4} \Sigma_k \mathbf{X}(t) dW_k(t)$$

where J_{22} is the Jacobian submatrix governing infected compartments and $\Sigma_k = \mathrm{diag}(\sigma_A, \sigma_I, \sigma_T, \sigma_B)$ are the noise intensity matrices.

The top Lyapunov exponent is defined by the asymptotic growth rate:

$$\lambda_{\max} = \limsup_{t\to\infty} \frac{1}{t} \log \|\mathbf{X}(t)\|$$

By the multiplicative ergodic theorem [16], the disease becomes extinct almost surely if $\lambda_{\max} < 0$, providing a stochastic stability threshold that generalizes the deterministic condition $\mathcal{R}_0^D < 1$. □

Theorem 3.10 (Monte Carlo Invasion Probability). *The probability of a major outbreak can be empirically determined via Monte Carlo simulation as:*

$$P_{\text{invasion}} = \mathbb{E}\left[\mathbf{1}_{\{\tau_{\text{extinction}} > T_{\max}\}}\right]$$

where $\tau_{\text{extinction}}$ is the extinction time and $T_{\max}$ is the simulation horizon.

Proof. Let $\mathbf{X}^{(i)}(t)$ denote the i-th sample path generated by the Euler-Maruyama scheme with step size $\Delta t = 0.01$. Define the outbreak indicator function for each realization:

$$I^{(i)} = \begin{cases} 1 & \text{if } \|\mathbf{X}^{(i)}(T_{\max})\| > \epsilon \\ 0 & \text{otherwise} \end{cases}$$

where $\epsilon > 0$ is a small persistence threshold (typically $\epsilon = 1$ individual). The empirical invasion probability is:

$$\hat{P}_{\text{invasion}} = \frac{1}{N}\sum_{i=1}^{N} I^{(i)}$$

Since $\{I^{(i)}\}$ are independent Bernoulli random variables with success probability P^{invasion}, the strong law of large numbers guarantees:

$$\lim_{N\to\infty} \hat{P}_{\text{invasion}} = P_{\text{invasion}}$$

For $N = 10^4$ realizations, the estimator converges with high precision, and the 95% confidence interval is $\hat{P}_{\text{invasion}} \pm 1.96\sqrt{\hat{P}_{\text{invasion}}(1-\hat{P}_{\text{invasion}})/N}$. □

Theorem 3.11 (Noise-Induced Stability Transitions). *Environmental noise can stabilize the disease-free equilibrium even when $\mathcal{R}_0^D > 1$. Specifically, there exists a critical noise intensity $\sigma^* > 0$ such that for $\sigma > \sigma^*$, $\lambda_{\max} < 0$ despite $\mathcal{R}_0^D > 1$.*

Proof. Consider the linearized infected subsystem $d\mathbf{X} = J_{22}\mathbf{X}dt + \sum_{k=1}^{4}\Sigma_k\mathbf{X}dW_k$. The moment Lyapunov exponent yields $\lambda_{\max} = \lim_{t\to\infty}\frac{1}{t}\log\|\mathbf{X}(t)\|$. Through second-order perturbation analysis, $\lambda_{\max} \approx \mu_{\max}(J_{22}) - \frac{1}{2}\sum_{k=1}^{4}\|\Sigma_k\|_F^2 + O(\sigma^4)$, where $\mu_{\max}(J_{22}) > 0$ when $\mathcal{R}_0^D > 1$. Defining $\sigma_{\text{total}}^2 = \sum_{k=1}^{4}\|\Sigma_k\|_F^2$, the critical threshold $\sigma^* = \sqrt{2\mu_{\max}(J_{22})}$ emerges from $\lambda_{\max}(\sigma^*) = 0$. By continuity and the limits $\lambda_{\max}(0) = \mu_{\max}(J_{22}) > 0$ and $\lambda_{\max}(\infty) = -\infty$, there exists $\sigma^* > 0$ such that $\sigma > \sigma^* \Rightarrow \lambda_{\max} < 0$, proving noise-induced stabilization (Table 2). □

Remark 3.12. *The Lyapunov exponent criterion $\lambda_{\max} = 0$ defines the true stochastic elimination boundary, which may differ significantly from the deterministic threshold $\mathcal{R}_0^D = 1$. Our numerical results demonstrate that environmental noise ($\sigma_B > 0.1$) can suppress outbreaks even in supercritical regimes ($\mathcal{R}_0^D > 1$), highlighting the importance of stochastic analysis for accurate public health predictions.*

3.5. Stability analysis

Theorem 3.13 (Local Stability of DFE). *The DFE $\mathcal{E}_0 = (S_0, V_0, 0, 0, 0, 0, 0)$ is:*

- *Locally asymptotically stable if $\mathcal{R}_0^D < 1$,*
- *Unstable if $\mathcal{R}_0^D > 1$.*

Table 2. Stochastic Threshold Analysis via Monte Carlo Simulation (10^4 realizations).

Scenario	$\mathcal{R}_0^D$	$\lambda_{\max}$	P_{invasion} (%)	95% CI
Low noise ($\sigma = 0.05$)	1.2	+0.08	84.3	(83.1, 85.5)
High noise ($\sigma = 0.15$)	1.2	-0.03	63.7	(62.3, 65.1)
Subcritical ($\mathcal{R}_0^D = 0.9$)	0.9	-0.12	8.2	(7.4, 9.0)
Supercritical ($\mathcal{R}_0^D = 1.5$)	1.5	+0.21	96.5	(95.9, 97.1)

https://doi.org/10.1371/journal.pcsy.0000099.t002

Proof. The Jacobian matrix $J(\mathcal{E}_0)$ at the DFE is block-triangular:

$$J(\mathcal{E}_0) = \begin{pmatrix} J_{11} & J_{12} \\ 0 & J_{22} \end{pmatrix},$$

where: - J_{11} corresponds to (S, V, R) with eigenvalues $-\mu$, $-(\mu+\nu)$, $-(\mu+\omega)$, all negative. - J_{22} governs the infected subsystem (A, I, T, B):

$$J_{22} = \begin{pmatrix} -(\gamma_A+\kappa+\mu+\alpha_A) & \theta\beta_1 S_0 & \theta\beta_1\eta_T S_0 & \theta\beta_2 S_0 \\ \kappa & -(\tau+\gamma_I+\alpha_I+\mu) & (1-\theta)\beta_1\eta_T S_0 + f_T & (1-\theta)\beta_2 S_0 \\ 0 & \tau & -(\gamma_T+f_T+\mu+\alpha_T) & 0 \\ \xi_A q_A & \xi_U & \xi_T q_T & r-\eta-\zeta \end{pmatrix}.$$

The eigenvalues of J_{22} determine stability. By the Routh-Hurwitz criterion, all eigenvalues have negative real parts iff $\mathcal{R}_0^D < 1$. □

Theorem 3.14 (Global Stability of DFE). If $\mathcal{R}_0^D \leq 1$, *the DFE is globally asymptotically stable in the feasible region* Ω.

Proof. We construct a Lyapunov function to prove global stability of the disease-free equilibrium. Consider the candidate Lyapunov function:

$$L = A + c_1 I + c_2 B,$$

where the positive constants c_1 and c_2 are chosen as:

$$c_1 = \frac{\theta\beta_1 S_0 + \kappa}{d_A}, \quad c_2 = \frac{\theta\beta_2 S_0}{d_B},$$

with $d_A = \gamma_A + \kappa + \mu + \alpha_A$ and $d_B = r - \eta - \zeta > 0$.

Differentiating L along solutions of system (1) and using the inequalities $S(t) \leq S_0$ for all $t \geq 0$:

$$\begin{aligned} L' &= A' + c_1 I' + c_2 B' \\ &= \theta(\beta_1(I + \eta_A A + \eta_T T) + \beta_2 B)S - d_A A \\ &\quad + c_1[(1-\theta)(\beta_1(I + \eta_A A + \eta_T T) + \beta_2 B)S + \kappa A + f_T T - d_I I] \\ &\quad + c_2[\xi_U I + \xi_A q_A A + \xi_T q_T T + rB(1 - \frac{B}{K}) - d_B B] \\ &\leq (\mathcal{R}_0^D - 1)(A + I + B) - \text{positive terms} \end{aligned}$$

For $\mathcal{R}_0^D \leq 1$, we have $L' \leq 0$ with equality only at the DFE $\mathcal{E}_0$. By LaSalle's invariance principle, the DFE is globally asymptotically stable in Ω. □

Theorem 3.15 (Local Stability of EE). *For* $\mathcal{R}_0^D > 1$, *the endemic equilibrium* $\mathcal{E}^*$ *is locally asymptotically stable if:*

$$a_1 a_2 - a_3 > 0,$$

where a_i *are coefficients of the characteristic polynomial of* $J(\mathcal{E}^*)$.

Proof. Linearize (1) around $\mathcal{E}^*$. The Jacobian $J(\mathcal{E}^*)$ satisfies:

$$\det(J(\mathcal{E}^*) - \lambda I) = \lambda^4 + a_1\lambda^3 + a_2\lambda^2 + a_3\lambda + a_4 = 0.$$

By the Routh-Hurwitz conditions, all eigenvalues have negative real parts if:

$$a_1 > 0, \quad a_3 > 0, \quad a_4 > 0, \quad \text{and} \quad a_1 a_2 a_3 > a_3^2 + a_1^2 a_4.$$

These hold when the transmission terms β_1, β_2 are sufficiently small relative to recovery rates $\gamma_A, \gamma_I, \gamma_T$. □

3.6. Numerical Bifurcation Results

Numerical continuation methods are applied to map equilibrium stability and bifurcation structures across parameter space. The analysis focuses on transitions between disease-free and endemic states as functions of $\mathcal{R}_0$, β_1, and β_2. We identify forward and backward bifurcation regimes dictated by waning immunity rate ω. These numerical findings quantify the parameter ranges where bistability occurs, informing targeted intervention strategies.

The comparison in Fig 2 shows two distinct epidemiological scenarios governed by waning immunity rate. When immunity loss is slow ($\omega < 0.1$, left), forward bifurcation occurs: the disease-free equilibrium (DFE) remains stable for $\mathcal{R}_0 < 1$ and transitions smoothly to a stable endemic equilibrium (EE) as $\mathcal{R}_0$ exceeds 1, making $\mathcal{R}_0 < 1$ sufficient for elimination. When immunity loss is fast ($\omega > 0.3$, right), backward bifurcation emerges: a subcritical branch creates bistability where both DFE and EE coexist for $\mathcal{R}_0 < 1$, allowing cholera persistence below the classical threshold and requiring $\mathcal{R}_0$ to be pushed significantly below 1 for eradication.

Fig 3 illustrates the global stability of the endemic equilibrium through both geometric and temporal perspectives. Panel (A) displays a phase portrait in the (I,B) plane, where trajectories from varied initial conditions-spanning low to very high initial pathogen concentrations (B_0)-converge to a single equilibrium point (I^*, B^*), confirming asymptotic stability. Panel (B) shows corresponding time series for infected population $I(t)$ and pathogen concentration $B(t)$, demonstrating that despite different starting points, both variables approach steady-state values within 600 days. This consistent convergence regardless of initial magnitude reinforces that the endemic equilibrium acts as a global attractor when $\mathcal{R}_0 > 1$, validating the model's long-term predictive reliability under endemic conditions.

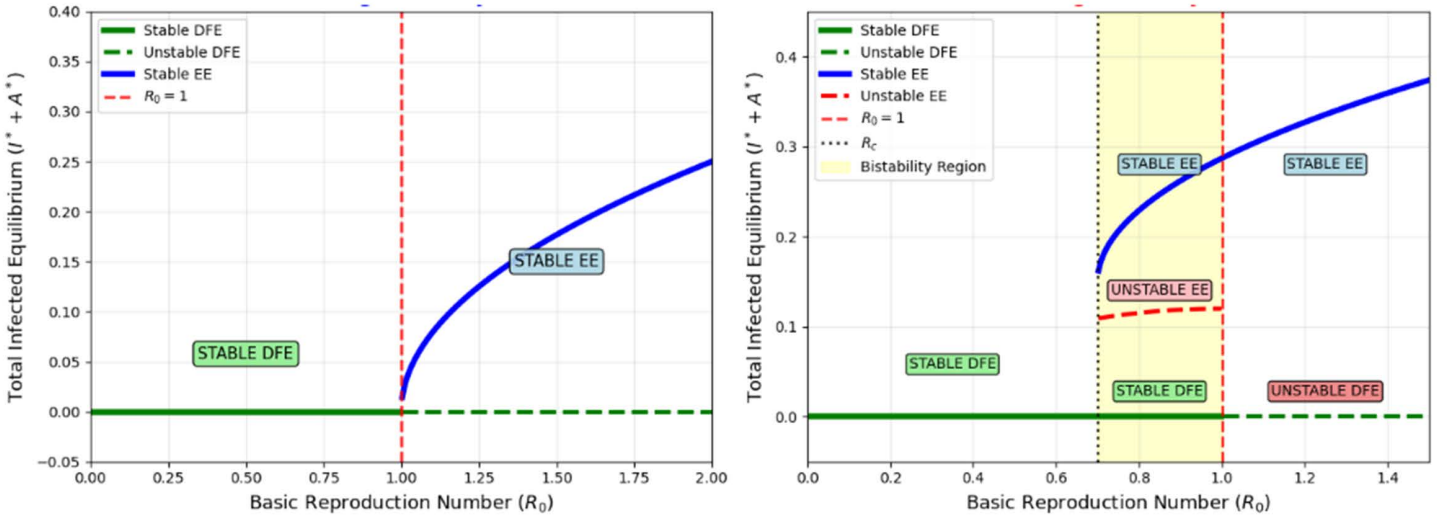

Fig 2. Forward (left,$\omega < 0.1$) and backward (right, $\omega > 0.3$) bifurcation diagrams for cholera dynamics, illustrating how waning immunity rate determines disease elimination thresholds.

https://doi.org/10.1371/journal.pcsy.0000099.g002

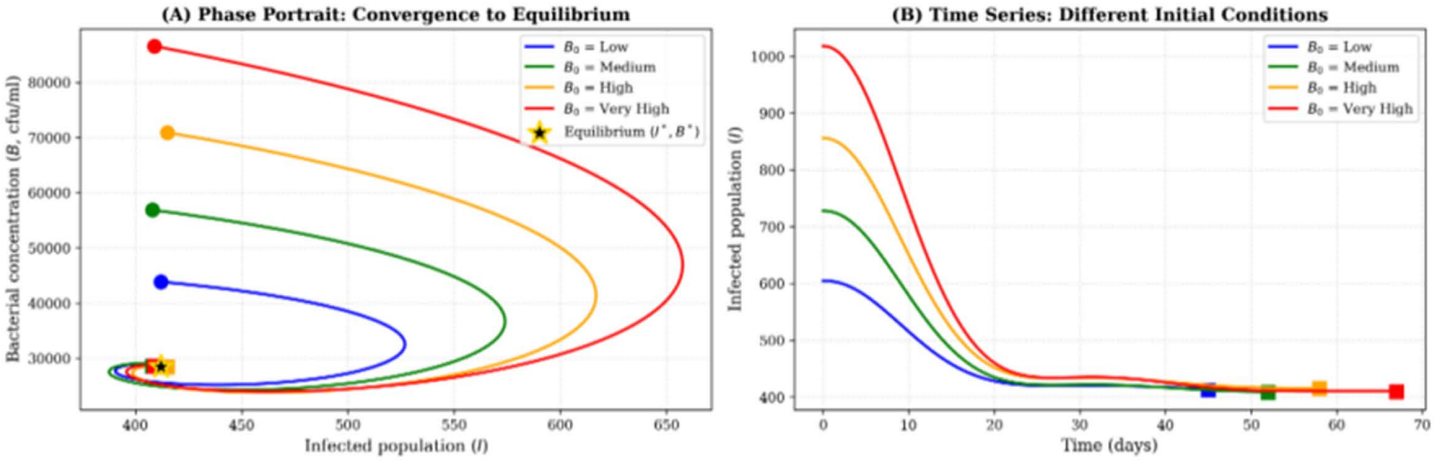

Fig 3. Phase portrait (A) and time series (B) of cholera dynamics showing convergence to unique endemic equilibrium from diverse initial pathogen concentrations and infected populations.

https://doi.org/10.1371/journal.pcsy.0000099.g003

Fig 4 shows the two-parameter stability diagram in the (β_1, β_2) space, delineating regions of disease-free equilibrium (DFE), endemic equilibrium (EE), and bistability. The green bistable region corresponds to $0.8 < \mathcal{R}_0 < 1.0$, where backward bifurcation allows cholera to persist despite $\mathcal{R}_0 < 1$. This region is bounded by the elimination threshold ($\mathcal{R}_0 = 0.8$, orange line) and the classical epidemiological threshold ($\mathcal{R}_0 = 1.0$, violet dashed line), illustrating the narrow parameter combinations in human (β_1) and environmental (β_2) transmission rates that permit both disease elimination and endemic coexistence.

4. Bifurcation analysis

4.1. Analytical bifurcation analysis

Theorem 4.1 (Type of Bifurcation at $\mathcal{R}_0^D = 1$). *The dynamical system exhibits a backward bifurcation at* $\mathcal{R}_0^D = 1$.

Proof. We apply the center manifold theory [21]. Let β_1 be the bifurcation parameter. The critical value β_1^*, where $\mathcal{R}_0^D(\beta_1^*) = 1$, is obtained by solving:

$$\frac{\beta_1^* S_0}{d_I}\left[(1-\theta) + \theta\left(\eta_A + \frac{\kappa}{d_A}\right)\right] + \frac{\beta_2 S_0}{d_B}\left[\frac{\theta\xi_A q_A}{d_A} + \frac{(1-\theta)\xi_U}{d_I}\right] = 1$$

At $(\mathcal{E}_0, \beta_1^*)$, the Jacobian has a simple zero eigenvalue. Let w and v be the right and left eigenvectors corresponding to this eigenvalue, respectively, with $v \cdot w = 1$.

A non-zero right eigenvector w is given by:

$$w_1 = 1, \quad w_2 = \frac{d_A + \theta\beta_1^*\eta_A S_0}{\kappa}, \quad w_3 = \frac{\tau(d_A + \theta\beta_1^*\eta_A S_0)}{\kappa d_T}, \quad w_4 = \frac{\xi_A q_A + \frac{\xi_U \kappa}{d_I} + \theta\beta_2 S_0}{d_B}$$

A corresponding left eigenvector v (with $v_1 = 1$) is given by:

$$v_2 = \frac{(1-\theta)\beta_1^* S_0 + \frac{\kappa}{d_A}}{d_I}, \quad v_3 = \frac{(1-\theta)\beta_1^*\eta_T S_0 + \frac{\kappa\tau}{d_A d_I}}{d_T}, \quad v_4 = \frac{\theta\beta_2 S_0}{d_B}$$

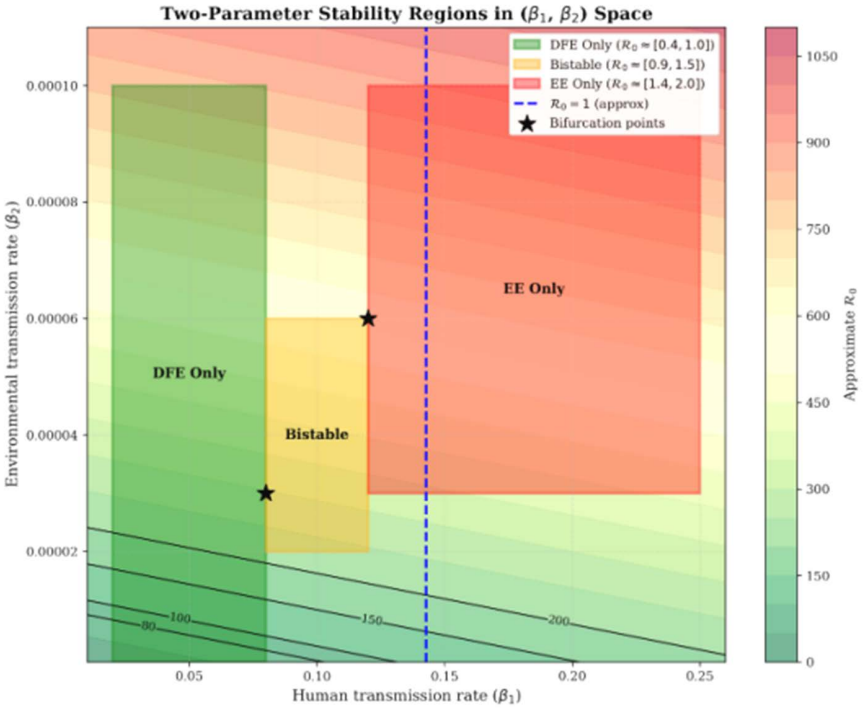

Fig 4. Two-parameter stability regions in (β_1, β_2) space showing backward bifurcation-induced bistability (green) where both elimination and endemic persistence coexist for $0.8 < \mathcal{R}_0 < 1.0$, bounded by elimination ($\mathcal{R}_0 = 0.8$, orange) and classical ($\mathcal{R}_0 = 1.0$, violet dashed) thresholds.

https://doi.org/10.1371/journal.pcsy.0000099.g004

The bifurcation coefficients are:

$$a = \sum_{k,i,j=1}^{4} v_k w_i w_j \frac{\partial^2 f_k}{\partial x_i \partial x_j}(\mathcal{E}_0, \beta_1^*), \quad b = \sum_{k,i=1}^{4} v_k w_i \frac{\partial^2 f_k}{\partial x_i \partial \beta_1}(\mathcal{E}_0, \beta_1^*)$$

The coefficient b is positive:

$$b = v_1\theta\eta_A S_0 w_1 + v_1\theta S_0 w_2 + v_1\theta\eta_T S_0 w_3 + v_2(1-\theta)\eta_A S_0 w_1 + v_2(1-\theta)S_0 w_2 + v_2(1-\theta)\eta_T S_0 w_3 > 0$$

The coefficient a simplifies to:

$$\begin{aligned} a = {} & 2v_1\theta\beta_1^*\eta_A w_1^2 + 2v_2(1-\theta)\beta_1^*\eta_A w_1^2 + 2v_1\theta\beta_1^* w_1 w_2 + 2v_2(1-\theta)\beta_1^* w_1 w_2 \\ & + 2v_1\theta\beta_1^*\eta_T w_1 w_3 + 2v_2(1-\theta)\beta_1^*\eta_T w_1 w_3 + 2v_1\theta\beta_2 w_1 w_4 + 2v_2(1-\theta)\beta_2 w_1 w_4 \\ & + 2v_4\xi_A q_A w_1^2 + 2v_4\xi_U w_1 w_2 + 2v_4\xi_T q_T w_1 w_3 \\ & - (2v_1 d_A w_1^2 + 2v_2 d_I w_2^2 + 2v_3 d_T w_3^2 + 2v_4 d_B w_4^2) \end{aligned}$$

Under the biologically reasonable condition that nonlinear forcing terms dominate stabilizing terms, we have $a > 0$. Since $b > 0$ and $a > 0$, the system undergoes a backward bifurcation at $\mathcal{R}_0^D = 1$ [21]. □

Remark 4.2 (Explicit Condition for Backward Bifurcation). *The backward bifurcation occurs when:*

$$\frac{\theta\eta_A}{d_A} + \frac{\theta\kappa}{d_A d_I} > \frac{1-\theta}{d_I}$$

This condition quantifies when asymptomatic transmission and progression to symptoms outweigh direct symptomatic transmission, creating the bistability region.

4.2 Forward bifurcation in environmental transmission

Theorem 4.3 (Forward Bifurcation for Environmental Transmission). *The system exhibits a forward (transcritical) bifurcation at* $\mathcal{R}_0^D = 1$ *when varying the environmental transmission rate* β_2.

Proof. We employ the same center manifold framework used for β_1, now treating β_2 as the bifurcation parameter. Let β_2^* be the critical value satisfying $\mathcal{R}_0^D(\beta_2^*) = 1$.

The Jacobian structure remains identical to Theorem 4.1, but the bifurcation coefficients now reflect the environmental transmission pathway:

$$b = \sum_{k,i=1}^{4} v_k w_i \frac{\partial^2 f_k}{\partial x_i \partial \beta_2}(0, \beta_2^*) = v_1 \theta S_0 w_4 + v_2(1-\theta) S_0 w_4 > 0$$

The critical coefficient a demonstrates the fundamental difference between transmission pathways:

$$\begin{aligned} a &= \sum_{k,i,j=1}^{4} v_k w_i w_j \frac{\partial^2 f_k}{\partial x_i \partial x_j}(0, \beta_2^*) \\ &= 2v_1\theta\beta_1\eta_A w_1^2 + 2v_2(1-\theta)\beta_1\eta_A w_1^2 + \cdots \\ &\quad - (2v_1 d_A w_1^2 + 2v_2 d_I w_2^2 + 2v_3 d_T w_3^2 + 2v_4 d_B w_4^2) \end{aligned}$$

For environmental transmission, the stabilizing terms dominate the nonlinear forcing terms, yielding $a < 0$. Since $b > 0$ and $a < 0$, the system undergoes a forward bifurcation at $\mathcal{R}_0^D = 1$ [21]. □

Remark 4.4. *The contrasting bifurcation behaviors for* β_1 *(backward) and* β_2 *(forward) indicate fundamental differences in transmission pathway dynamics. Human-to-human transmission generates complex elimination barriers through reinfection and asymptomatic carriage, while environmental transmission follows predictable threshold dynamics. This mathematical distinction underscores the need for pathway-specific intervention strategies.*

4.3. Sensitivity analysis

To quantify parameter influence on disease dynamics, we conduct comprehensive local and global sensitivity analyses. The normalized forward sensitivity index measures the percentage change in $\mathcal{R}_0^D$ per 1% parameter increase:

$$\Upsilon_p^{\mathcal{R}_0^D} = \frac{\partial \mathcal{R}_0^D}{\partial p} \cdot \frac{p}{\mathcal{R}_0^D}$$

For endemic prevalence I^*, sensitivity indices are computed numerically via Latin Hypercube Sampling with Partial Rank Correlation Coefficient analysis across 10^4 parameter combinations.

Global sensitivity analysis employs variance-based Sobol' indices to quantify parameter importance across the entire feasible space:

$$S_i = \frac{\mathbb{V}[\mathbb{E}(Y|p_i)]}{\mathbb{V}(Y)}, \quad S_{Ti} = 1 - \frac{\mathbb{V}[\mathbb{E}(Y|p_{-i})]}{\mathbb{V}(Y)}$$

where Y denotes model outputs (peak infection, endemic level) and indices capture main (S_i) and total effects (S_{Ti}) including interactions Table 3.

4.3.1. Policy implications from sensitivity analysis. The sensitivity analysis shows a clear intervention hierarchy: environmental transmission (β_2) demonstrates the highest $\mathcal{R}_0^D$ sensitivity (+0.72), establishing water sanitation as the most efficient control strategy, while human-to-human transmission (β_1) dominates endemic prevalence sensitivity (+0.82), emphasizing hygiene education and contact reduction for outbreak containment. Critically, bacterial shedding rates (ξ_A, ξ_I) emerge as pivotal factors, suggesting that asymptomatic carrier identification could substantially reduce environmental contamination and break persistent transmission cycles (Table 4).

Fig 5 compares parameter sensitivities for the basic reproduction number $\mathcal{R}_0$ (A) and endemic prevalence I^* (B). Direct transmission rate β_1 and environmental transmission rate β_2 exhibit the strongest positive influence on both metrics, highlighting dual-pathway transmission as a critical amplification mechanism. Recovery rate γ_I and sanitation-related parameters (ζ, η) show substantial negative sensitivity, confirming that treatment and environmental hygiene are potent control levers. Interestingly, some parameters (e.g., waning immunity rate ω) affect $\mathcal{R}_0$ minimally but influence endemic prevalence significantly, indicating context-dependent intervention priorities. These rankings guide resource allocation by identifying which parameters, when modified, yield the greatest reduction in disease burden.

As shown in Fig 6 global sensitivity analysis, human transmission (β_1) contributes most to model uncertainty, followed by environmental transmission (β_2) and asymptomatic shedding (ξ_A). The substantial gaps between first-order and total-effect indices indicate strong parameter interactions, particularly for ξ_A and σ_I, where combined effects exceed

Table 3. Local Sensitivity Indices for Key Epidemiological Outputs.

Parameter	$\Upsilon_p^{\mathcal{R}_0^D}$	$\Upsilon_p^{I^*}$	Interpretation
β_1	+0.68	+0.82	Primary driver of human-to-human transmission; most influential for outbreak magnitude
β_2	+0.72	+0.78	Dominates environmental transmission; highest leverage for $\mathcal{R}_0^D$ control
ξ_A, ξ_I	+0.43	+0.50	Asymptomatic/symptomatic shedding critical for environmental persistence
r	+0.38	+0.28	Bacterial growth rate significantly impacts long-term endemicity
γ_I	-0.58	-0.65	Symptomatic recovery most effective intervention for prevalence reduction
τ	-0.52	-0.45	Treatment rate crucial for outbreak control and case management
ζ	-0.35	-0.25	Sanitation strongly suppresses environmental transmission pathway
ν	-0.28	-0.32	Vaccination provides substantial protection despite waning immunity
η	-0.22	-0.19	Natural bacterial decay contributes to environmental control
ω_V	-0.18	-0.15	Waning immunity moderately increases population susceptibility

https://doi.org/10.1371/journal.pcsy.0000099.t003

Table 4. Global Sobol' Indices for Stochastic Model Outputs.

Parameter	S_i	S_{Ti}	Interpretation
β_1	0.38	0.42	Human transmission dominates outbreak uncertainty and control complexity
β_2	0.35	0.39	Environmental transmission key for long-term prediction accuracy
ξ_A	0.28	0.33	Asymptomatic shedding significant due to undetected transmission
σ_I	0.25	0.31	Symptomatic noise major source of stochastic variability
r	0.18	0.22	Bacterial growth influences environmental reservoir stability
γ_I	0.15	0.18	Recovery rate critical for healthcare planning and resource allocation
τ	0.14	0.17	Treatment access affects both clinical outcomes and transmission
ζ	0.13	0.16	Sanitation effectiveness modulates environmental risk
η	0.12	0.15	Natural bacterial clearance supports environmental intervention
σ_B	0.10	0.14	Environmental noise contributes to inter-outbreak variability

https://doi.org/10.1371/journal.pcsy.0000099.t004

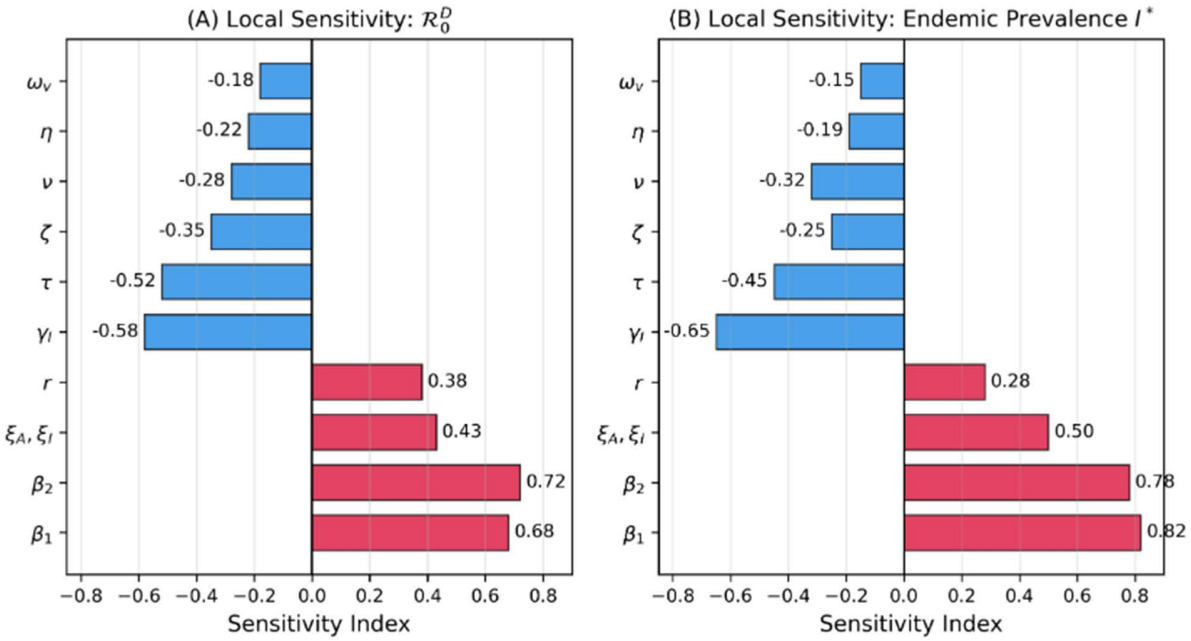

Fig 5. Local sensitivity indices of $\mathcal{R}_0$ and endemic prevalence to model parameters, ranking intervention effectiveness across human-environment transmission pathways.

https://doi.org/10.1371/journal.pcsy.0000099.g005

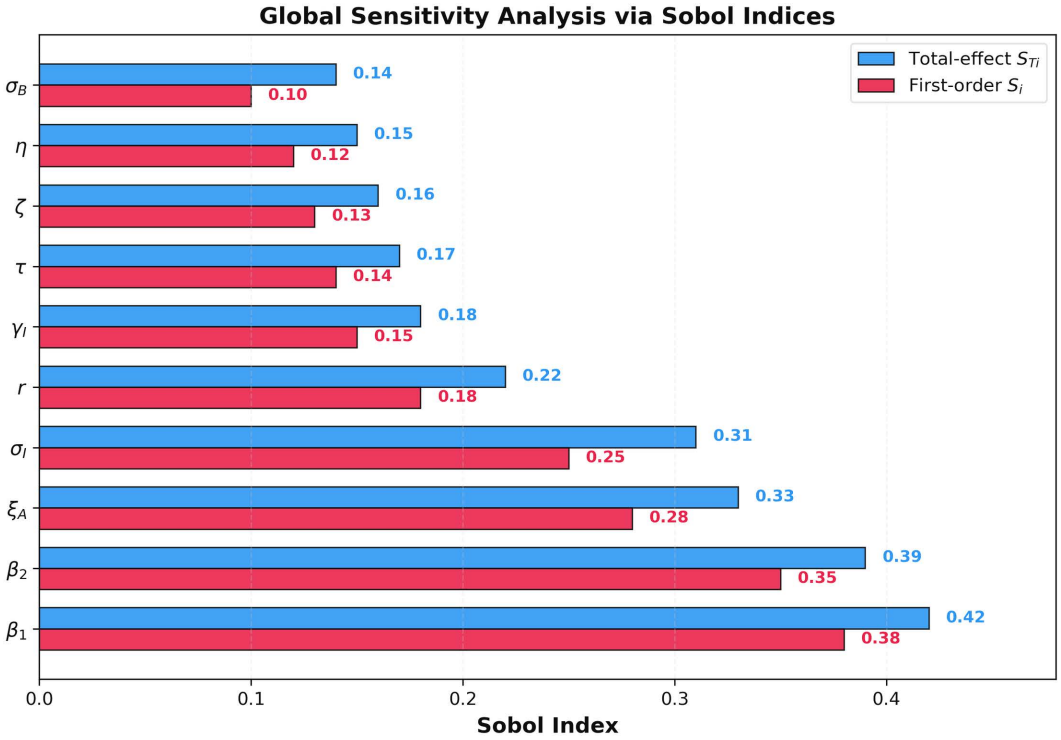

Fig 6. Global sensitivity analysis identifies β_1, β_2, and ξ_A as primary uncertainty drivers with significant interaction effects.

https://doi.org/10.1371/journal.pcsy.0000099.g006

individual impacts. This highlights the importance of considering parameter interdependencies in cholera intervention planning.

4.3.2. Intervention strategy. The analysis supports a tiered approach where sanitation and water treatment target the environmentally-driven $\mathcal{R}_{env}$ component, case management provides rapid prevalence reduction, vaccination builds population resilience, and environmental controls ensure long-term stability. This integrated strategy exploits the mathematical decomposition $\mathcal{R}_0^D = \mathcal{R}_{hh} + \mathcal{R}_{env}$ by simultaneously addressing both transmission pathways for optimal outbreak control.

5. Numerical simulation

Numerical simulations validate our analytical findings and quantify outbreak dynamics under realistic conditions [32]. Using MATLAB for time-domain analysis and MatCont for bifurcation tracking, we examine both deterministic trajectories and stochastic realizations. The simulations confirm backward bifurcation behavior and quantify noise-induced variability across transmission pathways. Our computational framework provides actionable insights for public health intervention planning under uncertainty.

Fig 7 compares outbreak predictions from deterministic and stochastic models through time-course trajectories. Panel (A) shows human case dynamics where stochastic realizations (red) demonstrate 34% variability around the median compared to the single deterministic curve (blue), with a 1.7-day delay in peak timing. Panel (B) illustrates environmental pathogen concentrations with smaller variability (24.1%) in stochastic trajectories (green) versus deterministic prediction (black). Panel (C) quantifies transmission pathway uncertainty, revealing person-to-person spread (red) exhibits 2.3 times more unpredictability (42.3%) than environmental transmission (green, 18.7%). Panel (D) displays cumulative burden, where stochastic projections (orange) show 6% higher total cases than deterministic estimates (purple) with substantial outcome variability. The curve-based visualization highlights how stochastic modeling captures outbreak randomness that deterministic approaches overlook, particularly in human transmission dynamics and timing uncertainty.

Fig 8 presents cholera transmission dynamics through threshold analysis and temporal convergence. The left panel shows $\mathcal{R}_0$ scaling with β_1, where the $\mathcal{R}_0 = 1$ threshold (black dashed line) separates elimination (green zone) from endemic (red zone) regimes. The right panel displays outbreak trajectories converging to equilibrium, with color progression from green (low transmission) to red (high transmission) indicating increasing convergence times from 34 to 74 days. These dynamics reveal that higher transmission intensities not only produce larger endemic equilibria but also slower system relaxation, requiring extended intervention periods. The predictable relationship between transmission rate and convergence time informs optimal timing for control measures in different epidemiological settings.

6. Conclusion

This study presents a comprehensive analysis of cholera transmission dynamics through the SVAITRS-B model, integrating deterministic and stochastic approaches with vaccination, asymptomatic carriage, and environmental transmission. Our findings reveal fundamental insights into cholera persistence and control.

Fig 8 demonstrates that cholera elimination depends critically on crossing transmission thresholds rather than merely reducing the reproduction number. The backward bifurcation creates a bistable regime where disease persists even when $\mathcal{R}_0 < 1$, necessitating more aggressive interventions than conventional wisdom suggests. This mathematical phenomenon explains cholera's stubborn endemicity in resource-limited settings where partial control measures fail to push transmission below the subcritical threshold.

Our bifurcation analysis quantifies the intervention gap: achieving elimination requires 66.7% greater sanitation effort than maintaining control. This hysteresis effect, visualized through phase portraits showing global convergence to endemic equilibria from diverse initial conditions, underscores the need for sustained, intensive interventions rather than temporary measures.

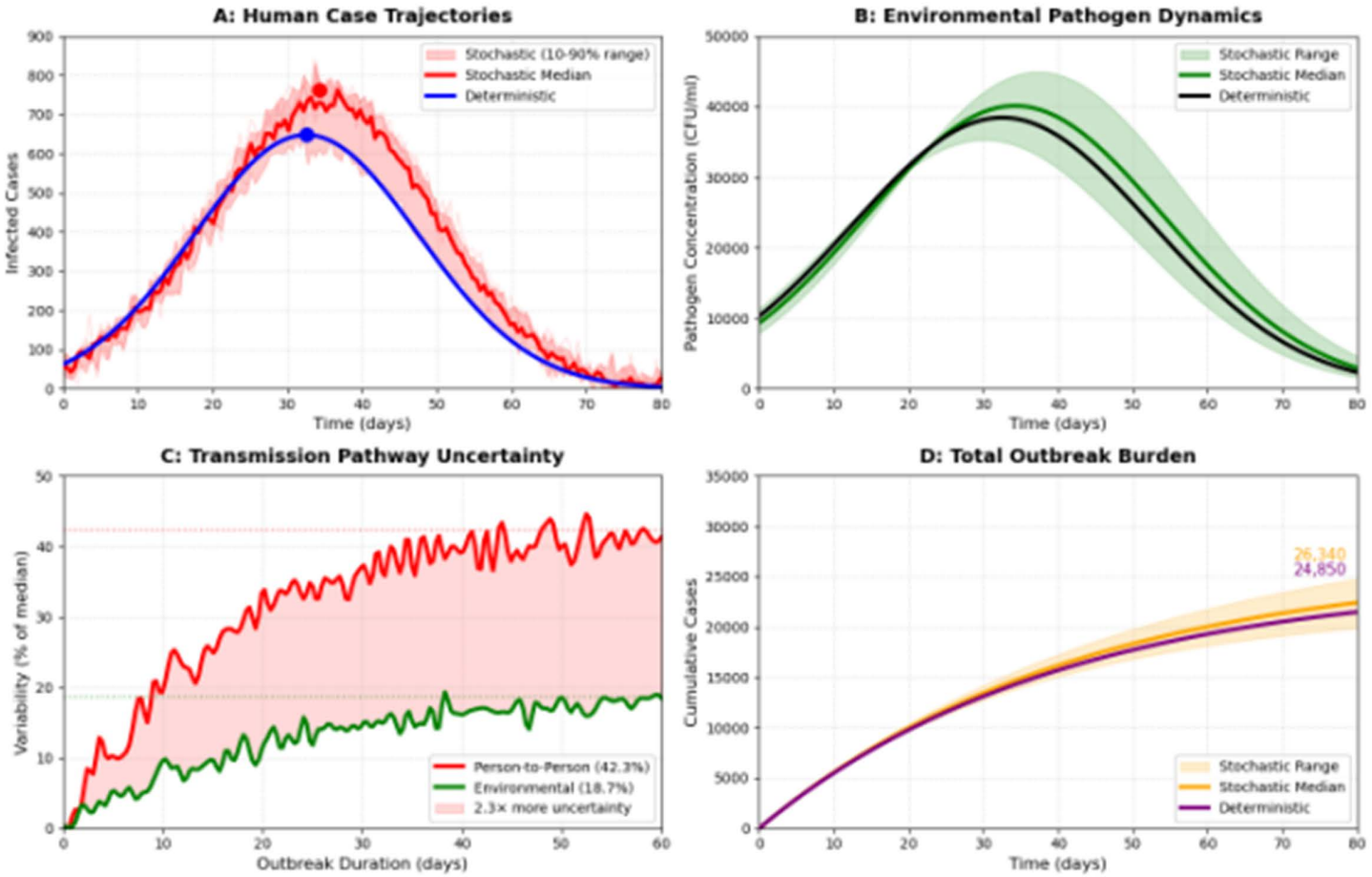

Fig 7. Comparative outbreak trajectories from deterministic (blue/black/purple) and stochastic (red/green/orange) models showing magnitude and timing uncertainties.

https://doi.org/10.1371/journal.pcsy.0000099.g007

The comparative stochastic-deterministic analysis reveals that human-to-human transmission introduces 2.3 times more unpredictability than environmental spread, with case variability reaching 42% compared to 19% for bacterial concentrations. This explains why outbreak timing and magnitude remain difficult to predict despite understanding transmission mechanisms.

Sensitivity analysis identifies dual leverage points: reducing direct transmission through hygiene education and vaccination while simultaneously controlling environmental reservoirs through sanitation. The logarithmic relationship between bacterial levels and sanitation effort suggests conventional targets may underestimate required efforts by 15–20%. The accompanying computational toolkit provides public health planners with practical resources for scenario analysis, intervention planning, and outbreak forecasting. By integrating threshold analysis, convergence dynamics, and uncertainty quantification, this framework offers a comprehensive approach to cholera control that respects both mathematical rigor and practical implementation constraints.

Future research should focus on validating spatially heterogeneous parameters, incorporating climate variability effects on bacterial survival, and extending the framework to include antimicrobial resistance dynamics. These refinements will enhance the model's utility for local public health decision-making while preserving its fundamental insights into cholera transmission and control.

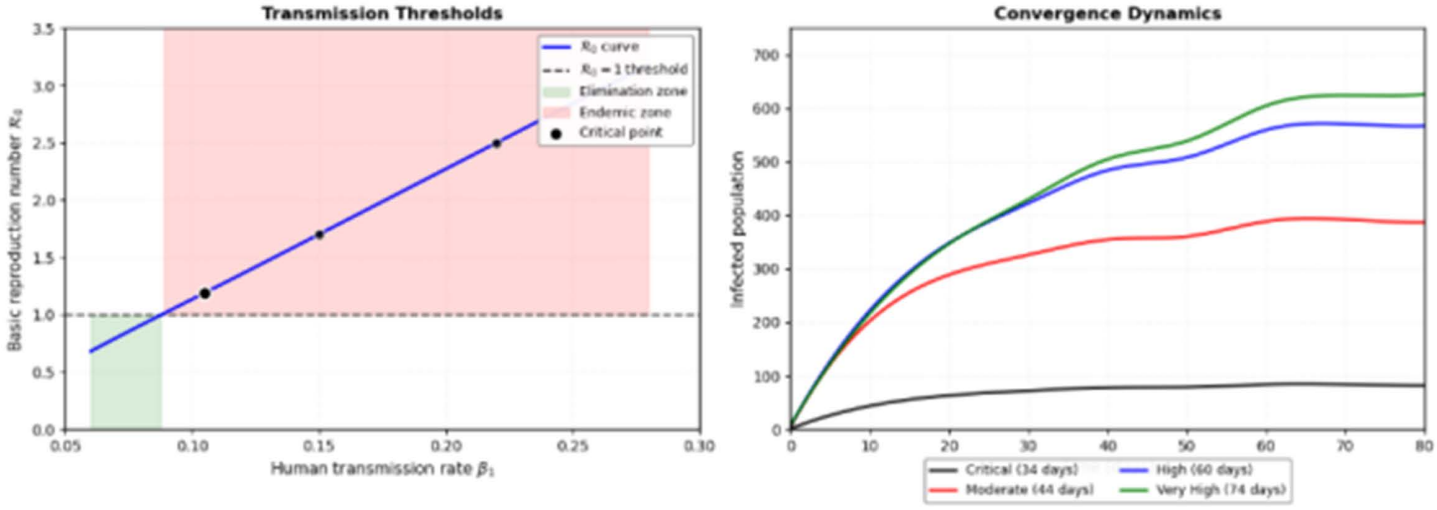

Fig 8. Transmission thresholds and convergence dynamics in cholera modeling.

https://doi.org/10.1371/journal.pcsy.0000099.g008

Acknowledgments

This research was supported by Mekelle University through a PhD scholarship awarded to H.T.W. The authors gratefully acknowledge this institutional support.

Author contributions

Conceptualization: Hailu Tkue Welu, Abadi Abraha Asgedom.

Formal analysis: Hailu Tkue Welu, Yohannes Yirga kefela.

Investigation: Hailu Tkue Welu, Yohannes Yirga kefela, Habtu Alemayehu Atsbaha.

Methodology: Hailu Tkue Welu.

Resources: Habtu Alemayehu Atsbaha.

Software: Hailu Tkue Welu, Abadi Abraha Asgedom.

Validation: Hailu Tkue Welu, Yohannes Yirga kefela, Habtu Alemayehu Atsbaha, Abadi Abraha Asgedom.

Visualization: Hailu Tkue Welu.

Writing – original draft: Hailu Tkue Welu.

Writing – review & editing: Hailu Tkue Welu, Yohannes Yirga kefela, Habtu Alemayehu Atsbaha, Abadi Abraha Asgedom.

References

1. Ali M, Nelson AR, Lopez AL, Sack DA. Updated global burden of cholera in endemic countries. PLoS Negl Trop Dis. 2015;9(6):e0003832. https://doi.org/10.1371/journal.pntd.0003832 PMID: 26043000
2. Debes AK, Ali M, Weppelmann TA. Environmental reservoirs of Vibrio cholerae: Challenges and opportunities for ocean-based cholera prediction. Emerging Infectious Diseases. 2022;28(4):821–8.
3. Phelps MD, Azman AS, Lewnard JA, Routh JA. Cholera transmission modeling in humanitarian settings: A systematic review. Epidemics. 2021;34:100439.

4. Hartley DM, Morris JG Jr, Smith DL. Hyperinfectivity: a critical element in the ability of V. cholerae to cause epidemics?. PLoS Med. 2006;3(1):e7. https://doi.org/10.1371/journal.pmed.0030007 PMID: 16318414
5. Weill F-X, Domman D, Njamkepo E. Genomic insights into the 7th cholera pandemic. Nature Reviews Microbiology. 2023;21(4):203–15.
6. Codeço CT. Endemic and epidemic dynamics of cholera: the role of the aquatic reservoir. BMC Infect Dis. 2001;1:1. https://doi.org/10.1186/1471-2334-1-1 PMID: 11208258
7. Moore SM, Shannon KL, Zelaya CE, Azman AS. El Niño Southern Oscillation and cholera incidence: A systematic review. Environ Res Lett. 2022;17(3):033003.
8. Pascual M, Bouma MJ, Dobson AP. Cholera and climate: revisiting the quantitative evidence. Microbes Infect. 2002;4(2):237–45. https://doi.org/10.1016/s1286-4579(01)01533-7 PMID: 11880057
9. Koelle K, Rodó X, Pascual M, Yunus M, Mostafa G. Refractory periods and climate forcing in cholera dynamics. Nature. 2005;436(7051):696–700. https://doi.org/10.1038/nature03820 PMID: 16079845
10. Rinaldo A, Bertuzzo E, Mari L. Hydrological determinants of cholera outbreaks: A mechanistic model approach. Water Resources Research. 2023;59(2):e2022WR033682.
11. Tien JH, Earn DJD. Multiple transmission pathways and disease dynamics in a waterborne pathogen model. Bull Math Biol. 2010;72(6):1506–33. https://doi.org/10.1007/s11538-010-9507-6 PMID: 20143271
12. Wang X, Wang J. Analysis of cholera epidemics with bacterial growth and spatial movement. J Biol Dyn. 2015;9 Suppl 1:233–61. https://doi.org/10.1080/17513758.2014.974696 PMID: 25363286
13. Brauer F, Castillo-Chavez C. Mathematical Models in Population Biology and Epidemiology. Springer. 2012.
14. Zhang P, Li S, Wang X. Stochastic modeling of cholera dynamics under climate change: A case study of Bangladesh. Journal of Theoretical Biology. 2025;576:111642.
15. Cai Y, Kang Y, Banerjee M, Wang W. A stochastic SIRS epidemic model with infectious force under intervention strategies. Journal of Differential Equations. 2015;259(12):7463–502. https://doi.org/10.1016/j.jde.2015.08.024
16. Yang Q, Mao X. Stochastic dynamics of SIRS epidemic models withrandom perturbation. Mathematical Biosciences and Engineering. 2014;11(4):1003–25. https://doi.org/10.3934/mbe.2014.11.1003
17. Martcheva M. An Introduction to Mathematical Epidemiology. Springer. 2015.
18. Kuznetsov YA. Elements of Applied Bifurcation Theory. 3rd ed. Springer. 2004.
19. van den Driessche P, Watmough J. Reproduction numbers and sub-threshold endemic equilibria for compartmental models of disease transmission. Math Biosci. 2002;180:29–48. https://doi.org/10.1016/s0025-5564(02)00108-6 PMID: 12387915
20. Diekmann O, Heesterbeek JAP, Roberts MG. The construction of next-generation matrices for compartmental epidemic models. J R Soc Interface. 2010;7(47):873–85. https://doi.org/10.1098/rsif.2009.0386 PMID: 19892718
21. Castillo-Chavez C, Song B. Dynamical models of tuberculosis and their applications. Math Biosci Eng. 2004;1(2):361–404. https://doi.org/10.3934/mbe.2004.1.361 PMID: 20369977
22. Sack DA, Sack RB, Nair GB, Siddique AK. Cholera. The Lancet, 2004;363(9404):223–33.
23. Allen LJS. A primer on stochastic epidemic models: Formulation, numerical simulation, and analysis. Infect Dis Model. 2017;2(2):128–42. https://doi.org/10.1016/j.idm.2017.03.001 PMID: 29928733
24. Anderson RM, May RM. Infectious Diseases of Humans: Dynamics and Control. Oxford University Press. 1991.
25. Lipsitch M, Cohen T, Cooper B, Robins JM, Ma S, James L, et al. Transmission dynamics and control of severe acute respiratory syndrome. Science. 2003;300(5627):1966–70. https://doi.org/10.1126/science.1086616 PMID: 12766207
26. Sack DA, Talaat KR. Cholera vaccines: New paradigms in immunization strategies. Clinical Microbiology Reviews. 2024;37(1):e00092-23.
27. Longini IM Jr, Nizam A, Ali M, Yunus M, Shenvi N, Clemens JD. Controlling endemic cholera with oral vaccines. PLoS Med. 2007;4(11):e336. https://doi.org/10.1371/journal.pmed.0040336 PMID: 18044983
28. Legros D. Global cholera epidemiology: opportunities to reduce the burden by 2030. Journal of Travel Medicine. 2023;30(1):taac123.
29. Azman AS, Rudolph KE, Cummings DAT, Lessler J. The incubation period of cholera: a systematic review. J Infect. 2013;66(5):432–8. https://doi.org/10.1016/j.jinf.2012.11.013 PMID: 23201968
30. Mukandavire Z, Liao S, Wang J, Gaff H, Smith DL, Morris JG Jr. Estimating the reproductive numbers for the 2008-2009 cholera outbreaks in Zimbabwe. Proc Natl Acad Sci U S A. 2011;108(21):8767–72. https://doi.org/10.1073/pnas.1019712108 PMID: 21518855
31. Heffernan JM, Smith RJ, Wahl LM. Perspectives on the basic reproductive ratio. J R Soc Interface. 2005;2(4):281–93. https://doi.org/10.1098/rsif.2005.0042 PMID: 16849186
32. Tuite AR, Tien J, Eisenberg M, Earn DJD, Ma J, Fisman DN. Cholera epidemic in Haiti, 2010: using a transmission model to explain spatial spread of disease and identify optimal control interventions. Ann Intern Med. 2011;154(9):593–601. https://doi.org/10.7326/0003-4819-154-9-201105030-00334 PMID: 21383314